Journal of Sound and Vibration (1998) **214**(3), 395–412
Article No. sv971513

FORCED RESPONSE ANALYSIS IN TIME AND FREQUENCY DOMAINS OF A TUNED BLADED DISK WITH FRICTION DAMPERS

G. Csaba

Linköping University, *Department of Mechanical Engineering/Division of Machine Design*, *S*-581 83 *Linköping*, *Sweden*

(*Received* 19 *September* 1997)

A micro-slip model of a friction damper is presented in this paper. There are two formulations derived from the original force and displacement functions of the damper: a numerical blade-to-blade model and a linearized blade-to-ground model. The numerical friction damper was used in a time domain simulation of the forced response of a beam–damper system under travelling wave excitation. Frequency domain simulations with one blade and the blade-to-ground damper were also carried out. Simulation results agree well, except around the optimal damper weight, which is the weight that minimizes the response amplitude of the blade and damper system. Results from frequency domain simulations give a lighter optimal damper weight than the time domain simulations. This leads to the conclusion that if frequency domain simulations are used to find the optimum damper weight, then a slightly heavier damper weight should be chosen than suggested by frequency domain results. Comparison between a microslip and a macroslip model for the friction interface shows that the macroslip model gets close to predicting the optimal weight, but the response level is much higher than when the microslip model was used.

1. INTRODUCTION

High cycle fatigue of turbine and compressor blades is one of the main problems with jet engines in service and is mostly caused by blade vibration resonance within the operating range of the engine. Friction dampers of the mass type and more especially platform dampers, shown in Figure 1, are frequently used by jet engine designers. It is a well know fact that friction dampers may reduce the vibratory blade response at resonance. There is, however, a lack of theoretical models that can predict the performance of an actual damper. A good background and review of the subject of friction damping of turbine blade vibration has been given by Griffin [1].

There are two theoretical approaches for the contact interface between blade and damper, the macroslip and the microslip models. The most commonly used is the macroslip approach, where the entire interface is either stuck or is sliding. The onset of sliding is governed by Coulomb's law of friction. The greatest advantage of the macroslip theory is that it is quite straightforward compared with microslip theory. In the microslip approach the elasticity of members in contact is included, which leads to a slip zone that will gradually extend inward through the damper before the interface reaches macroslip. This is a more physically motivated method to use since normal forces are high and displacements are small in blade vibration.

Analysis has so far mostly been done on bladed disk systems, by using a simple macroslip damper model [2], or by using a more advanced microslip damper model on a

0022–460X/98/280395 + 18 $30.00/0

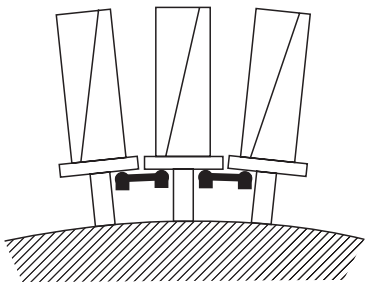

Figure 1. A part of a bladed disk with friction dampers.

simple structure [3, 4]. A microslip model has been described by Menq *et al*. [5] and applied in finding the response of a single-degree-of-freedom system. A microslip model which is derived from the Menq *et al*. model has been presented by Csaba [6].

The centrifugal force on the damper gives the normal load between blade and damper and the damping effect arises from the relative motion between damper and blade platform. The damper connects two adjacent blades via friction joints. This means that the damper displacement is found through the relative motion of the baldes. This damper type is called a blade-to-blade damper, (BB-damper).

Systems with Coulomb friction, i.e., friction dampers, are inherently non-linear. Computer simulations are faster if the damper properties are linearized. The harmonic balance method, HBM, is the most commonly used linearization method in friction damping analysis. A thorough discussion of HBM may be found in reference [6]. The accuracy of HBM may be found by comparing the frequency domain solution with the time marching solution for the forced response of a blade–damper system. Simulations by Menq and Griffin [7] and Csaba [6] show good agreement for a one-blade, one-damper system where the damper was attached to a fixed point and a moving point, i.e., the beam. This damper type is called a blade-to-ground damper, (BG-damper). Sinha and Griffin [8, 9] have shown that if one considers a tuned bladed disk fitted with macroslip BB-dampers linearized by harmonic balance, then the steady state response may be found by using a single blade and an equivalent BG-damper.

One objective in this paper is to present an improvement of the microslip model in reference [6] to incorporate both micro- and macroslip and to present a model of an actual damper as shown in Figure 2. Another objective is to investigate if equivalence between BB- and BG-dampers also holds for a microslip friction damper. This will be done by comparing time-marching results using multiple blades and microslip BB-dampers with steady state results using a single blade and an equivalent BG-damper linearized with HBM.

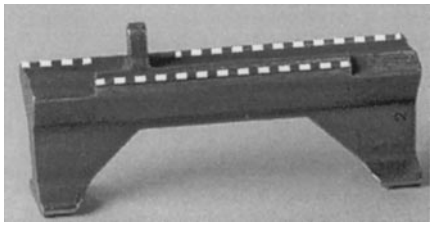

Figure 2. Photo of a commercially used damper. Broken white lines indicate contact interface.

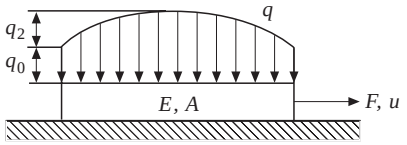

Figure 3. Microslip model for the friction interface.

2. FRICTION INTERFACE MODEL

To model the friction interface between the blade platform and the damper contact point, the microslip friction model developed by Csaba [6], shown in Figure 3 is used. This model, which is derived from the Menq *et al*. [5] one-bar model, is as simple as possible, but yet complete enough to show the most important properties of a microslip friction interface. The friction interface is modelled by a rectangular bar pressed against a rigid surface with a normal load q. The displacement of the bar end and the force are defined as u and F respectively. The bar has a modulus of elasticity E, and a cross-section area A. The length of the bar is l. The normal load is defined by using the quadratic function $q(x) = q_0 + 4q_2(xl - x^2)/l^2$. The friction force is defined by using Coulomb's friction law and a coefficient of friction, μ, which is constant across the contact surface: $F_f(x) = \mu q(x)$. *A list of notation is given in an Appendix*.

2.1. MICRO-SLIP EQUATIONS

Force and displacement functions have been derived by Csaba [6]; only the results are presented here. It was found convenient to express these functions as functions of the amount of slip, Δ, in the interface, where $\Delta = 0$ means no slip and $\Delta = 1$ means that the interface is on the verge of macroslip. The force function for initial loading is

$$F_i(\Delta_i) = \mu l \Delta_i (q_0 + q_2(2\Delta_i - \tfrac{4}{3}\Delta_i^2)). \tag{1}$$

The displacement function for initial loading of the bar end is

$$u_i(\Delta_i) = (\mu l^2 \Delta_i^2 / EA)(q_0/2 + q_2(\tfrac{4}{3}\Delta_i - \Delta_i^2)). \tag{2}$$

The state of the friction joint is defined by the initial loading. The force amplitude, F_i, and displacement, u_i, are defined by equations (1) and (2) respectively for a given initial slip coefficient Δ_i. Force and displacement for cyclic motion are then governed by the so called Massing rules, see reference [5] or [10]. These rules states that the hysteresis curve for unloading and reloading, F_u, u_u and F_r, u_r respectively may be found by scaling the initial loading curve by a factor of two. Massing rules agree exactly with force and displacement functions derived by Csaba [6] where these rules were not used. The broken curve in

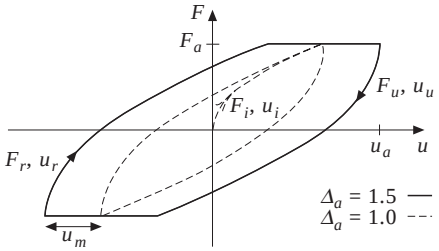

Figure 4. Hysteresis curves for micro- and micromacroslip.

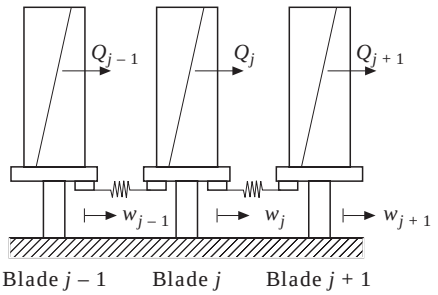

Figure 5. Definition of forces and displacements, for analysis of blade j.

Figure 4 shows the initial loading curve and a hysteresis curve when $\Delta_i = 1$, i.e., the interface is on the verge of macroslip.

2.2. FORCE AND DISPLACEMENT FOR MICRO-MACRO-SLIP

One can now extend force and displacement functions to allow for macroslip during part of the loading cycle. It is assumed that a given displacement, u, is applied to the interface. The displacement function is monotonic between its peak values, with an amplitude, u_a, which is large enough to give macroslip in the interface.

There will be both micro- and macroslip motion of the interface. For every time the displacement changes direction, the interface will start with microslip until the slip coefficient is $\Delta = 1$. The force has now reached its peak value, the whole interface starts to slide, i.e., one has macroslip. The macroslip motion stops when the displacement changes direction again. The micro-macroslip motion is shown in Figure 4 as the solid line hysteresis curve.

The macroslip displacement of the interface is defined by a variable, u_m. This displacement is found as the difference between the displacement amplitude and the initial displacement that gives macroslip:

$$u_m = u_a - u_i(1). \tag{3}$$

The unloading and reloading displacement functions for micro- and macroslip are then found by using Massing rules by combining equation (3) with equation (2) and setting $\Delta_i = 1$. The force is equal to the limiting friction force during macroslip, and thus independent of the displacement.

It may be of interest to compare different micro-macroslip curves. A slip variable is therefore defined as

$$\Delta_a = u_a/u_i(1). \tag{4}$$

The solid line curve in Figure 4 show a plot where, $\Delta_a = 1{\cdot}5$. This means that the displacement amplitude is 1·5 times as large as required to cause macroslip of the interface.

3. BLADE-TO-BLADE FRICTION DAMPER MODEL

In this section a model will be derived of an actual blade-to-blade microslip friction damper. The damper model will then be converted into a numerical model and a BG-damper model for use in time and frequency domain simulations respectively.

It is assumed that the blade, denoted as blade j, shown in Figure 5, is part of a tuned bladed disk. Dampers that connect blade j to its neighbouring blades are denoted as dampers j-1 and j.

Figure 2 is a photo of an actual friction damper. There are three friction joints, indicated by broken white lines, connecting the two adjacent blades. A model of this damper is shown in Figure 6. The model consists of two friction interfaces, and a spring between them. The spring stiffness, k_d may for example be found from a finite element model of the physical damper.

The friction damper model in Figure 6 is chosen because it is the simplest model that takes into account the elastic deformation of the actual damper, and can simulate a BB-damper with micro- and macroslip. Unfortunately there is no direct coupling between the geometry of the actual damper and the friction interface parameters, A and l. These parameters have to be determined *ad hoc*. Data used here are: $EA = 1{\cdot}82\ MN$, $l = 3\ \mu m$, $\mu = 0{\cdot}5$, $k_d = 236\ N/\mu m$.

3.1. FORCE ON BLADE PLATFORM FROM BLADE-TO-BLADE DAMPERS

It is assumed that the two friction interfaces between blades and the damper are identical and thus have the same deformation,

$$u_1(\Delta) = u_2(\Delta) = u(\Delta). \tag{5}$$

Using equation (5) gives the displacement of the damper, v, as

$$v(\Delta) = 2u(\Delta) + F(\Delta)/k_d. \tag{6}$$

If the displacement is known, then the damper force is found from equation (1) in combination with equation (6) by iterating the slip coefficient Δ.

Assuming that the excitation on the blades is harmonic and of an engine order type, one can define the excitation force as

$$Q_j(t) = Q_a \sin(\omega t + j\varphi) \tag{7}$$

If EO is the engine order of excitation and n is the number of blades on the disk, then the interblade phase angle is found as

$$\varphi = 2\pi EO/n. \tag{8}$$

If one assumes also that the dampers are tuned, all blades will have the same response amplitude, but different interblade phase angles. The response at the platform may be written as

$$w_j(t) = w_a f(\omega t + j\varphi + \beta), \tag{9}$$

where $f(\omega t + j\varphi)$ is the response function with its phase angle, w_a is the response amplitude and β is a general phase angle. For simplicity, the deformation of the blade platform between damper contact points is neglected. Displacement of the damper is then found as the relative motion between its connecting blades.

$$v_{j-1}(t) = w_j(t) - w_{j-1}(t). \tag{10}$$

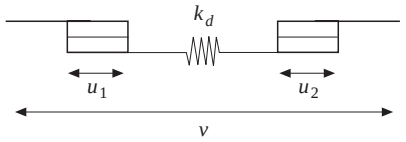

Figure 6. Model of an actual friction damper.

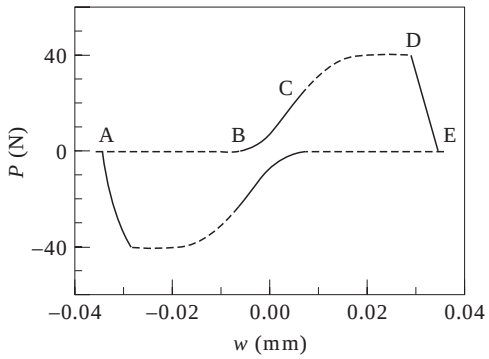

Figure 7. Hysteresis curve for the platform, $\varphi = 45^\circ$, $\Delta_a = 5$.

The damper force corresponding to displacement v_j is F_j found from equation (6). The total force on the platform of blade j from connecting friction dampers is then

$$P_j(t) = F_{j-1}(t) - F_j(t). \tag{11}$$

3.2. HYSTERESIS FOR THE BLADE PLATFORM

In this section it is assumed that the platform displacement, w, is given and the platform force, P, is to be computed. Force and displacement functions from section 2.2 can be used for the friction joint if displacements are monotonic between their peak values. The platform force is then found by iteration, where the variable is the slip coefficient Δ. The iteration procedure to find P_j is as follows: platform displacements w_{j-1}, w_j and w_{j+1} are given. Equation (10) gives v_j and v_{j-1}. Damper forces F_j and F_{j-1} are found by iterating Δ in equation (6). Platform force P_j is then given by equation (11).

Figure 7 shows a hysteresis curve for the blade platform and Table 1 shows the state for the two dampers connecting the blade to its neighbours. The state regions correspond to Figure 7 and are tabulated for half a cycle of motion. There are three states of slip during the motion: AB, where both dampers have macroslip, BC and DE, where one damper has macroslip and the other has microslip. The third state is CD, where both dampers have microslip. Region CD will eventually disappear if the displacement amplitude increases enough. Region AB will on the other hand disappear as the displacement decreases. Regions BC and DE will then disappear and there will be only microslip motion if the slip coefficient is less than unity.

It is important to note the region AB for the case shown. The force on the platform is zero in this region, due to the fact that the forces from the two dampers are equal, but acting in opposite directions. This means that there is no power input from the blade, but both dampers have macroslip, and are thus dissipating energy. This means that they are

TABLE 1

State of dampers during half a cycle of micro-macro-slip motion

Region	Damper $j-1$	Damper j
A–B	macroslip	macroslip
B–C	microslip	macroslip
C–D	microslip	microslip
D–E	macroslip	microslip

dissipating energy from a neighbouring blade. This may be seen as energy that is travelling through the bladed system.

4. LINEARIZATION

In this secton the non-linear platform hysteresis curve will be compared with the linearized ones. The harmonic balance method, HBM, is the most commonly used linearization method in friction damping analysis. Only the basic concept of the method will be reviewed here. A more thorough discussion can be found in reference [6]. There will be a non-linear response to a harmonic excitation for a non-linear system. The response may be expanded as a Fourier series. In HBM one assumes that the first sine and cosine terms of the Fourier expansion dominate, and all higher order terms are neglected. The benefit of using HBM is that non-linear differential equations that describe the blade–damper system are simplified into non-linear algebraic equations, which are solved faster.

There are two methods for doing this linearization: one either assumes the displacement to be harmonic and Fourier expands the force, or *vice versa*. In the present case one has a restriction on the traction force: the force may not exceed the limit friction force. It is therefore assumed that the displacement is harmonic and the force is linearized.

4.1. LINEARIZATION OF PLATFORM FORCE

There are two ways to linearize the platform force. One may assume the *platform displacement* w to be harmonic and linearize the platform force, here called HBM1 or assume the *friction interface displacement* u to be harmonic and linearize the traction force on the interface, here called HBM2. One starts by assuming harmonic platform displacement, HBM1. Equation (9) may then be written as

$$w_j(\theta) = w_a \sin(\omega t + j\varphi + \beta) = w_a \sin(\theta), \tag{12}$$

Neighbouring platforms have displacement

$$w_{j-1}(\theta) = w_a \sin(\theta - \varphi), \qquad w_{j+1}(\theta) = w_a \sin(\theta + \varphi). \tag{13, 14}$$

The total force from dampers on the platform may then be expressed by using linearized stiffness and damping functions which makes the computer code more efficient than if the linearized force were used directly. The linearized properties are found as

$$k_{P_{eq}}(\Delta_a, \varphi) = \frac{1}{\pi w_a} \int_{-\pi}^{\pi} P \sin\theta \, \mathrm{d}\theta, \qquad c_{P_{eq}}(\Delta_a, \varphi) = \frac{1}{\pi w_a} \int_{-\pi}^{\pi} P \cos\theta \, \mathrm{d}\theta. \tag{15, 16}$$

One should observe that the force in equations (15) and (16) is found by iteration as described in section 3.2. The friction interface is now described by a spring, k_{eq}, and a damper, c_{eq}, where the linearized properties are functions of slip coefficient amplitude, Δ_a, and interblade phase angle φ. The linearized traction force can then be expressed as

$$P_{eq}(\Delta_a, \varphi, \theta) = k_{P_{eq}}(\Delta_a, \varphi) w_a \sin\theta + c_{P_{eq}}(\Delta_a, \varphi) w_a \cos\theta. \tag{17}$$

The resulting linearized hysteresis curve is shown as curve HBM1 in Figure 8 where it is compared with the original non-linear hysteresis curve.

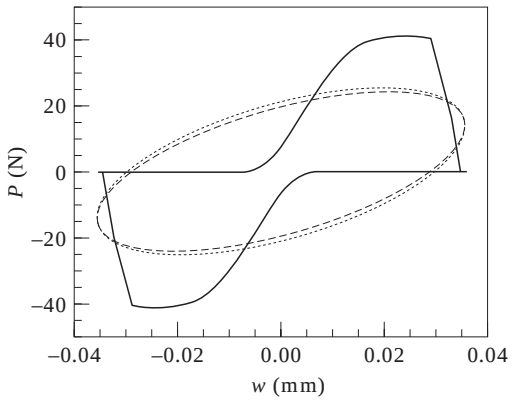

Figure 8. Non-linear and linearized hysteresis curves, $\varphi = 23^\circ$, $\Delta_a = 5$. —, Non-linear; - - - -, HBM1; · · · ·, HBM2.

4.2. LINEARIZATION OF FRICTION INTERFACE TRACTION FORCE

Here the friction interface displacement is assumed to be harmonic:

$$u(\theta) = u_a(\Delta_a) \sin \theta. \tag{18}$$

Applying HBM to the friction interface traction force gives the equivalent stiffness and damping functions as

$$k_{I_{eq}}(\Delta_a) = \frac{1}{\pi u_a(\Delta_a)} \int_{-\pi}^{\pi} F \sin \theta \, \mathrm{d}\theta, \qquad c_{I_{eq}}(\Delta_a) = \frac{1}{\pi u_a(\Delta_a)} \int_{-\pi}^{\pi} F \cos \theta \, \mathrm{d}\theta. \tag{19, 20}$$

It is notable that the equivalent stiffness and damping are functions of amplitude slip coefficient, but not the interblade phase angle which was the case when HBM1 was applied to the platform force. The equivalent traction force is then

$$F_{eq}(\Delta_a, \theta) = k_{I_{eq}}(\Delta_a) u_a(\Delta_a) \sin \theta + c_{I_{eq}}(\Delta_a) u_a(\Delta_a) \cos \theta. \tag{21}$$

One needs to establish the relationship between the friction interface displacement and platform displacement in order to compare hysteresis curves for the two linearization methods. Equations (18) and (21) in equation (6) give the damper displacement as a function of interface properties:

$$v(\Delta_a, \theta) = u_a(\Delta_a)[(2 + k_{I_{eq}}(\Delta_a)/k_d) \sin \theta + (c_{I_{eq}}(\Delta_a)/k_d) \cos \theta]. \tag{22}$$

Equations (12) and (13) in equation (10) give the damper displacement as a function of platform displacement:

$$v_j(\theta) = w_a[(1 - \cos \varphi) \sin \theta + \sin \varphi \cos \theta]. \tag{23}$$

Equations (22) and (23) should be equal and this gives the amplitude slip coefficient Δ_a. The resulting hysteresis curve is shown as HBM2 in Figure 8. From these curves one can see that the first harmonic component in HBM is not enough to describe the exact hysteresis curve. One method of comparing the linear systems to the exact non-linear is to compute the damping energy per cycle of motion, W: $W_{Nonlin} = 2{\cdot}162 \times 10^{-3}$ J/cycle, $W_{\mathrm{HBM1}} = 2{\cdot}864 \times 10^{-3}$ J/cycle, $W_{\mathrm{HBM2}} = 2{\cdot}713 \times 10^{-3}$ J/cycle.

The difference in damping energy is about 33% for the first and 26% for the second method of linearization compared with the exact damping energy, for this particular case. It was observed by plotting curves for different phase angles that the difference in damping

energy increases with smaller phase angles, and that the linearized damper always gives too much damping. Comparing the two methods of linearization with each other shows that the difference in damping energy is small, and either one may be used. There is, however, a benefit in computation time when using the HBM2 method. This is due to the fact that the platform has to be integrated numerically for varying interblade phase angle and displacement amplitude in HBM1, while the interface force is only numerically integrated for varying displacement amplitude in HBM2.

4.3. EQUIVALENT BLADE-TO-GROUND DAMPER MODEL

Griffin and Sinha [9] have shown that the response of a bladed disk with multiple blade and BB-damper elements agrees well with the response of a system with a single blade and an equivalent blade-to-ground damper. The model that they used was a one-degree-of-freedom model for the blade and damper model consisting of a macroslip element in series with a spring. Sinha and Griffin [8] showed that equivalence between a BB-damper and a BG-damper is found if

$$k_{\mathrm{BG}} = 4k_{\mathrm{BB}} \sin^2(\varphi/2), \qquad \mathrm{FS}_{\mathrm{BG}} = 2\mathrm{FS}_{\mathrm{BG}} \sin(\varphi/2). \tag{24, 25}$$

For the macroslip damper FS is the limiting friction force and k is the stiffness of the spring. In this section equations will be derived that give equivalence between BB- and BG-damper for the micro-macroslip damper described in this paper.

Using HBM2 one may express the linearized friction interface as a complex stiffness k_I^*,

$$k_I^*(\Delta_a) = k_{I_{eq}}(\Delta_a) + \mathrm{i}c_{I_{eq}}(\Delta_a). \tag{26}$$

The BB-damper is now described by two friction interfaces, each having a complex stiffness k_I^*, in series with the elastic damper stiffness k_d, as shown in Figure 9.

The resulting stiffness of this BB-damper is

$$k_{\mathrm{BB}}^*(\Delta_a) = k_I^*(\Delta_a)k_d/[2k_d + k_I^*(\Delta_a)]. \tag{27}$$

Using equation (27) one may write the damper force as a function of the damper displacement:

$$F^* = k_{\mathrm{BB}}^*(\Delta_a)v. \tag{28}$$

The force on the platform from a BG-damper is defined as

$$P^* = k_{\mathrm{BG}}^* w. \tag{29}$$

Next one needs to establish the relationship between damper and platform force and also damper and platform displacement. It is in this case more convenient to express platform displacements in equations (12)–(14) by using complex notation:

$$w_{j-1}^* = \hat{w}\,\mathrm{e}^{\mathrm{i}(\theta-\varphi)}, \qquad w_j^* = \hat{w}\,\mathrm{e}^{\mathrm{i}\theta}, \qquad w_{j+1}^* = \hat{w}\,\mathrm{e}^{\mathrm{i}(\theta+\varphi)}. \tag{30–32}$$

Equations (30)–(32) in equation (10) give the damper displacement as

$$v_{j-1}^* = \hat{w}\,\mathrm{e}^{\mathrm{i}\theta}(1 - \mathrm{e}^{-\mathrm{i}\varphi}), \qquad v_j^* = \hat{w}\,\mathrm{e}^{\mathrm{i}\theta}(\mathrm{e}^{\mathrm{i}\varphi} - 1). \tag{33, 34}$$

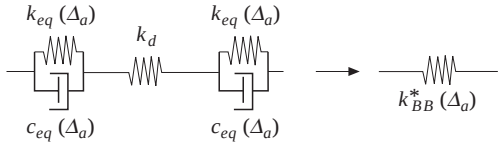

Figure 9. Linearized model of a damper.

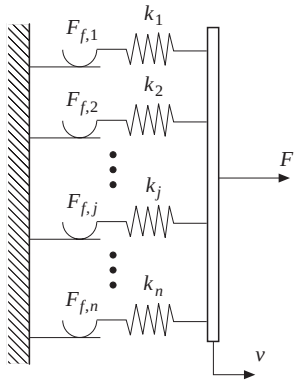

Figure 10. Parallel–series model of a friction damper.

Equations (33) and (34) in equation (28) give the damper forces, which with equation (11) will give the platform force as

$$P_f^*(\Delta_a, \varphi) = k_{\mathrm{BB}}^*(\Delta_a)\hat{w}\, \mathrm{e}^{\mathrm{i}\theta}(2 - \mathrm{e}^{-\mathrm{i}\varphi} - \mathrm{e}^{\mathrm{i}\varphi}). \tag{35}$$

Comparing equation (35) with equation (29) gives equivalent blade-to-ground stiffness, after simplification, as

$$k_{\mathrm{BG}}^*(\Delta_a, \varphi) = 4k_{\mathrm{BB}}^*(\Delta_a)\sin^2(\varphi/2). \tag{36}$$

Evidently equation (36) agrees exactly with equation (24). The difference is that the BG-stiffness for the micro-macroslip damper is a function not only of interblade phase angle but also of amplitude slip coefficient.

The best way to see if the linearization is acceptable is to compare the forced response for a system where k_{eq} and c_{eq} are used with the response for a system where the original nonlinear damper equations are used. This is the topic of the following sections of this paper.

4.4. NUMERICAL DAMPER MODEL

Force and displacement functions must be able to vary arbitrarily in a transient time domain simulation. It is possible to find the damper force for a given arbitrary displacement, by using Massing rules, but it is not efficient when computation time is considered. Instead, a numerical damper model based on the parallel–series model by Iwan [10] has been developed. The model has been used by Wettergren and Csaba [11] and Wettergren [12], to simulate dynamic instability in a turbine generator due to microslip. A similar model has also been used by Sanliturk and Ewins [13]. The model is here extended to incorporate macroslip.

The parallel–series model, shown in Figure 10, consists of a number of macroslip elements in parallel forming a microslip element. The force–displacement relationship is described by

$$F(v) = \sum_{j=1}^{n'} s_j F_{f,j} + \sum_{j=n'+1}^{n} k_j(v - v_{0,j}), \tag{37}$$

where the summation from 1 to n' includes all elements that are slipping, and the summation from $n' + 1$ to n includes all elements that remain elastic after loading. Stiffness k_i and limiting friction force $F_{f,j}$ are found from initial loading functions equation (1) and

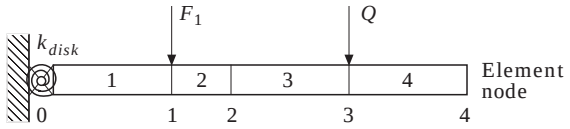

Figure 11. Beam model of a blade.

equation (2). This formulation has two new features, a state vector s, and a displacement vector v_0. The direction of the friction force is saved in s_j as element j starts to slip. The displacements of all slipping elements are saved in v_0, and n' is set to zero when the time derivative of the damper displacement, $\dot{v}$ changes sign. These two features allow for an arbitrary displacement function and a combination of both macro- and microslip.

5. BLADED DISK MODEL

A simplified blade model as shown in Figure 11 was used for simulations. It consists of four elements where element 1 represent the blade neck, 2 the platform, 3 and 4 the airfoil of the blade. A torsion spring with stiffness, k_{disk} connects the blade to the disk, which is considered as rigid ground. Dampers are attached at node 1, represented by force F_1. The blade is excited at node 3, force Q. Three criteria were established for equivalence between the full FE-model and the beam model: (a) the same first natural frequency, f_n; (b) the same mode shape for the first natural frequency; (c) the total mass should be the same.

Natural frequencies and mode shape for the first flexural frequency were computed for the full FE-model. Results are shown in Table 2 and Table 3. The second column corresponds to simulations where a spring with stiffness k_d is attached at node 1. This gives a crude estimation of how well the two models agree for a locked damper, i.e., no slip in the contact interface.

TABLE 2

Natural frequencies for FE and beam models

	FE model		Beam model	
Mode	f_n (Hz)	f_n, locked (Hz)	f_n(Hz)	f_n, locked (Hz)
1F	1079	1221	1077	1242
2F	4746	5110	4960	5527

† A spring with stiffness k_d is attached at node 1.

TABLE 3

Mode shape at first natural frequency for FE and beam models

	FE model		Beam model	
Node	ψ	ψ, locked	ψ	ψ, locked
1	0·0543	0·0266	0·0528	0·0321
2	0·0988	0·0651	0·0978	0·0676
3	0·4813	0·4627	0·4866	0·4500
4	1	1	1	1

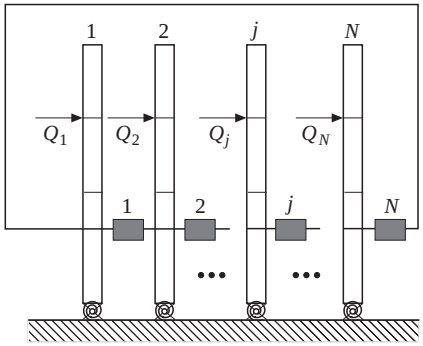

Figure 12. A blade-damper system connected to a rigid disk.

Parameters, i.e., beam height and width, and attachment stiffness k_{disk} were varied to get the best fit for the 1F frequency and mode shape. The results are also shown in Tables 2 and 3. Comparing the results, one sees that there is good enough agreement for the present purpose between the full FE-model and the beam model.

6. FORCED RESPONSE SIMULATION

Griffin and Sinha [9] have shown that the response of a bladed disk with multiple blade and BB-damper elements agrees well with the response of a system with a single blade and an equivalent BG-damper. The models they used were a one-degree-of-freedom model for the blade and a damper model consisting of a macroslip element in series with a spring. They assumed harmonic motion in both simulation cases. This section is concerned with investigating whether the equivalence also holds for a micro-macroslip damper, but harmonic motion is not assumed for the BB-damper case.

The damper–blade system that was used for simulations is shown in Figure 12. It consists of N blades and dampers. Each damper, shown as a grey box, is attached to two blades, the last damper being connected to the last and the first blade, as shown in Figure 12. It is assumed that the excitation is in the form of a travelling wave. This implies that the number of blades needed for the analysis is $N = 2\pi/\varphi$, where φ is called the interblade phase angle. The excitation force is then $Q_j(t) = \hat{Q}\, e^{i(\omega t - j\varphi)}$, where $\hat{Q}$ is the amplitude.

A computer code was developed to analyze the system. Basic features are: mass and stiffness matrix for one blade are imported from the finite element program used in section 3. The frequency domain solution is used as initial value for the time domain simulation.

6.1. FREQUENCY DOMAIN SIMULATION

It is not necessary to use the complete N-blade-damper system to find the frequency domain solution. This is due to the fact that all blades are tuned and thus have the same

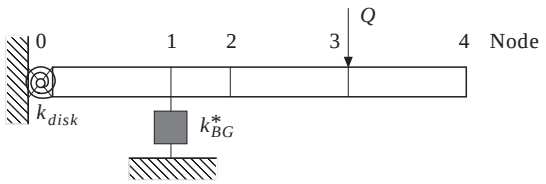

Figure 13. Blade-damper system used in frequency-domain simulation.

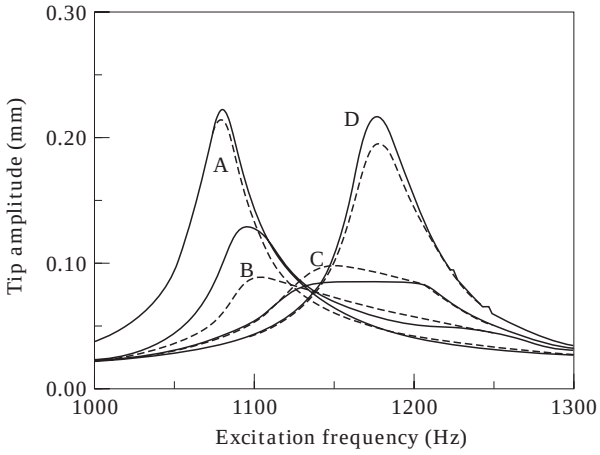

Figure 14. Amplitude tip displacement versus excitation frequency for damper mass 5 m, 10 m, 20 m and 100 m. Simulation with $N = 8$ blades. A, 5 m; B, 10 m; C, 20 m; D, 100 m. ——, Time; - - - , frequency.

response. Instead the computer program uses one blade and a blade-to-ground damper, as shown in Figure 13.

The governing equation is

$$[\mathrm{M}]\{\ddot{x}\} + [\mathrm{C}]\{\dot{x}\} + [\mathrm{K}]\{x\} = \{Q\}. \tag{38}$$

The damping matrix is generated by using Rayleigh damping:

$$[\mathrm{C}] = \alpha[\mathrm{M}] + \beta[\mathrm{K}]. \tag{39}$$

Coefficients α and β are chosen to give the assumed value of 1% modal damping at the first resonance frequency for the blade. One may either choose a value for α and then compute β, or the other way around. The damping matrix represents other types of damping in the system, apart from the contribution from the platform damper. The complex damper stiffness, k^*_{BG} is then assembled into the blade matrix. This gives a system stiffness matrix [K*] which is complex. Harmonic excitation and displacement are assumed:

$$\{Q^*\} = \{\hat{Q}^*\}\, \mathrm{e}^{\mathrm{i}\omega t}, \qquad \{x^*\} = \{\hat{x}^*\}\, \mathrm{e}^{\mathrm{i}\omega t} \tag{40, 41}$$

Equations (38)–(41) give the response as

$$\{\hat{x}^*\} = ([\mathrm{K}^*] + \mathrm{i}\omega[\mathrm{C}] - \omega^2[\mathrm{M}])^{-1}\{\hat{Q}\}. \tag{42}$$

For every ω, equation (42) is solved by an iterative procedure, where the slip coefficient Δ_a has to be found. It was shown in section 4.3 that for a given amplitude of blade platform displacement, the relative motion of two adjacent blades, i.e., the damper displacement, is as given by equation (34). This equation may be expressed as

$$v_0(\Delta_a, \varphi) = 2|\hat{x}_1^*| \sin(\varphi/2), \tag{43}$$

where $|\hat{x}_1^*|$ and v_0 are platform and damper amplitude displacements respectively. Thus equation (42) is solved by iterating the slip coefficient Δ_a so that equation (43) is in equilibrium.

6.2. TIME DOMAIN SIMULATION

The N-blade–damper system is used in the time domain simulation. The governing equations are equations (38), (39) and (40), where equation (38) is rewritten as a first order

ODE to suit the time domain solver. The response is found by exciting at a given frequency and then using direct time integration until steady state is reached.

These simulations tend to take a long time. The time and frequency response are fairly close, at most excitation frequency values, as shown in Figure 14. The frequency domain response is therefore used as initial value in the time domain simulation. This was shown to be quite effective and reduced computation time considerably.

7. NUMERICAL RESULTS

Simulations were made for $N = 8$, 13 and 19 blades, which correspond to interblade phase angles $\varphi = 45^\circ$, $27{\cdot}7^\circ$ and $18{\cdot}9^\circ$ respectively. The main effect of varying the number of blades is on the damper stiffness, which is also indicated by equation (36). Figure 14 show results from the $N = 8$ simulation. Simulations with $N = 13$ and 19 gave essentially the same response curves, but with less shift in resonance frequency as the damper is loaded. These simulation results are not presented here.

The most characteristic parameter in friction damper design is the normal force on the friction interface. The normal force is found from the centripetal acceleration of the damper mass which is induced by the rotor speed. One should note that the damper normal load is therefore frequency dependent and it is more accurate to use the damper weight as a parameter rather than the normal load on the interface.

7.1. COMPARISON OF TIME AND FREQUENCY DOMAIN RESULTS

Response plots for simulations with a given excitation force, Q and varying damper mass 5 m, 10 m, 20 m, and 100 m are shown in Figure 14. These simulations and corresponding response curves are denoted from A to D as shown in the plot legend. The plot shows tip deflection, i.e., $|\hat{x}_4^*|$ versus excitation frequency. It can be seen that the resonance frequency increases with the damper weight. It is furthermore seen that there is an optimal damper weight which minimizes the overall response, but more than five response curves

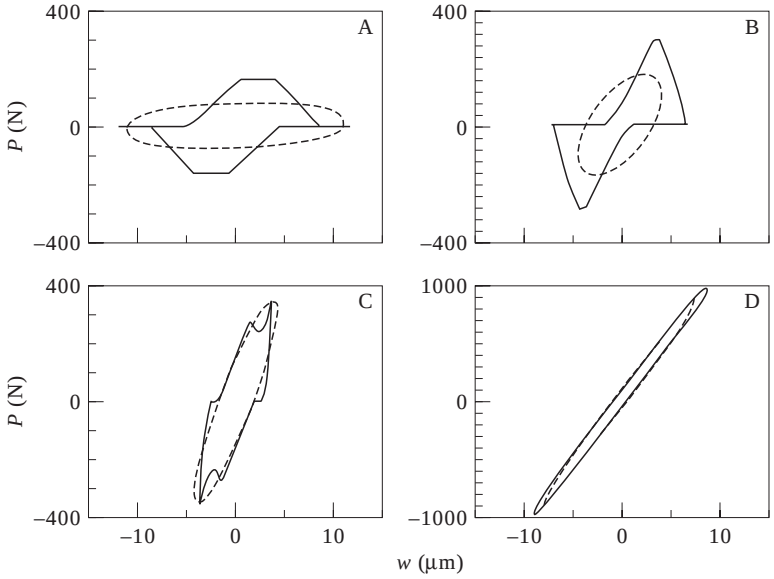

Figure 15. Hysteresis loop at resonance amplitude for simulations A, B, C, D representing damper mass 5 m, 10 m, 20 m, 100 m. Key as Figure 14.

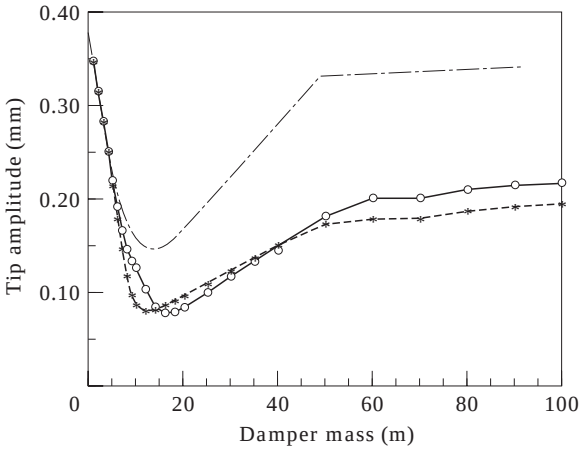

Figure 16. Tip displacement at resonance versus damper mass. Micro- and macroslip simulations in time and frequency domain. Simulation with $N = 8$ blades. – · – · , Macro; ○–○, time; -★-★-★-, frequency.

are needed to determine what optimum weight is. One sees also in Figure 14 that frequency and time domain solutions agree well for high and low damper weights, but not as well for weights around the optimal.

7.2. COMPARISON OF HYSTERESIS CURVES AT RESONANCE

Hysteresis plots for the platform, node 1, are shown in Figure 15. The platform displacement, w is plotted versus the force from the dampers on the platform, P. One sees in Figure 14 that simulations A, B and D give a higher response in the time domain, while simulation C gives a lower response. Figure 7 in section 3.2 shows a hysteresis curve that was plotted upon assuming that the displacement is harmonic and then computing the corresponding damper force. Comparing Figure 7 with time domain hysteresis for simulations A and B in Figure 15 shows close resemblance. It was found in section 4.2. that the linearized damper gives higher damping energy than the non-linear one for a given amplitude displacement. This can also be seen in Figure 14, for simulations A and B. The difference between time and frequency response is greater for simulation B simply because a heavier damper has more effect on blade response.

Simulation D in Figure 14 shows good agreement between time and frequency solutions. This is shown in Figure 15 where the solid curve is almost elliptic. It can also be seen in this figure that there is little friction damping in this simulation, which is indicated by the enclosed area of the hysteresis curve. The damper works more as a stiffener than a friction damper in this simulation.

The appearance of the time domain hysteresis curve for simulation C is somewhere in between curve B and D. The overall shape is fairly elliptic, but there are force harmonics of higher order seen in the plot. This can also be found by Fourier expanding the response displacement and the damper force on the platform. It appears that energy is dissipated due to higher harmonics so that the peak amplitude in Figure 14 is lower in the time domain solution than in the frequency domain solution.

7.3. OPTIMAL DAMPER WEIGHT

The optimal damper weight, i.e., the weight that minimizes the blade response over the frequency range of interest, is found by plotting response maximum against the friction damper weight, as shown in Figure 16. This figure shows results for time and frequency

domain simulations with the microslip damper model. There is also a dotted curve showing results with the same damper model except that the microslip interface model has been replaced by a macroslip model. This was done to highlight the difference in response results between the two interface models.

Comparing results from time and frequency domain simulations shows that they agree well. There is however less agreement near the optimal damper weight which is 12 m and 16 m for time and frequency domain results respectively. The difference in weight is about 25%, which one may consider acceptable, but a more important difference is that the frequency domain simulation gives a lighter optimal damper weight than the time domain simulation does. If one assumes results from time domain simulations to be more accurate but uses frequency domain simulations to find the optimum damper weight, then one should choose a weight that is slightly heavier than suggested by frequency domain results. One should also note that the gradient of the displacement curve is large on the left hand side of the optimal point. It is interesting to note that the response at optimal damper weight is approximately the same for time and frequency simulations. Comparing results obtained with the microslip model and results from using a standard macroslip interface model shows that the latter model gives higher response levels, but approximately the same optimal damper weight.

7.4. COMPARISON WITH SIMILAR WORK

Csaba [6] and Menq and Griffin [7] have done simulations with one blade, modelled with beam elements, and one blade-to-ground damper. Both papers showed very good agreement between time and frequency domain solutions. The present work shows that the agreement is not so good when the microslip blade-to-blade damper is loaded near the optimal weight. This was not observed in references [6] and [7]. One may also note that the response curve is flattened around resonance in reference [7] for high normal loads, while this paper shows more distinctive peaks at resonance. This is due to the fact that in reference [7] a macro-slip model was used, which locks up for high normal loads, while there is still slip in a microslip model.

8. CONCLUSIONS

A microslip model of an actual friction damper has been developed in this paper. There are two formulations of the damper derived from the original force and displacement functions of the damper: a numerical blade-to-blade model for simulations in the time domain and a linearized blade-to-ground model for simulations in the frequency domain, where the complex equivalent stiffness of the damper is derived by applying the harmonic balance method to the non-linear force from a given harmonic displacement.

Results show that hysteresis curves using original force and displacement functions and curves using the linearized model give about 30% difference in damping energy, where the linearized damper always gives too much damping.

The numerical friction damper was used in time domain simulation of the forced response of a beam–damper system under travelling wave excitation. Frequency domain simulations with one blade and a blade-to-ground damper were also carried out. Results from these two simulation methods were compared.

Comparison of the two methods shows that they agree well, except around the optimal damper weight, which is the weight that minimizes the response amplitude of the blade and damper system. Results from frequency domain simulations give a lighter optimal damper weight than simulations in time domain. This leads to the conclusion that if

frequency domain simulations are used to find the optimum damper weight, then a slightly heavier damper weight should be chosen than suggested by frequency domain results.

Comparison between using a microslip and a macroslip model for friction interface shows that the macroslip model gets close in predicting the optimal weight, but the response level is much higher than when the microslip model was used.

The final conclusion is that tuned disk simulations with a one-blade and a blade-to-ground damper may be used to get a crude estimation of the optimal weight for the friction damper and simulations in the time-domain can be used to get complementary results.

ACKNOWLEDGMENT

The author wishes to thank Magnus Andersson, Volvo Aero Corp., for providing data for the beam model and for fruitful discussions. This work is part of the research project "Friction Damping of Blade Vibrations", and is supported by the National Aeronautical Research Program under Grant NFFP-244.

REFERENCES

1. J. H. Griffin 1990 *International Journal of Turbo and Jet Engines* **7**, 297–307. A review of friction damping of turbine blade vibration.
2. A. Muszynska, D. I. G. Jones 1983 *Journal of Sound and Vibration* **86**, 107–128. On tuned bladed disk dynamics: some aspects of friction related mistuning.
3. K. Y. Sanliturk, M. Imregun and D. J. Ewins 1995 *Transactions of ASME*, *Journal of Vibration and Acoustics*, in press. Harmonic balance vibration analysis of turbine blades with friction dampers.
4. G. Csaba 1995 *Journal of Machine Vibration* **4**, 2–7. Friction damping of turbine blade vibrations using a microslip model.
5. C.-H. Menq, J. Beilak and J. H. Griffin 1986 *Journal of Sound and Vibration* **107**, 279–293. The influence of microslip on vibratory response, part I: a new microslip model.
6. G. Csaba 1995 *LiU-Tek-Lic*-1995:09, ISBN 91-7871-507-5, Linköping University, Sweden. Microslip friction damping, with special reference to turbine blade vibrations.
7. C.-H. Menq and J. H. Griffin 1985 *Transactions of ASME*, *Journal of Vibration*, *Acoustics*, *Stress and Reliability in Design* **107**, 19–25. A comparison of transient and steady state finite element analyses of the forced response of a frictionally damped beam.
8. A. Sinha and J. H. Griffin 1985 *AIAA Journal* **23**, 262–270. Effects of friction dampers on aerodynamically unstable rotor stages.
9. J. H. Griffin and A. Sinha 1985 *ASME Journal of Engineering for Gas Turbines and Power* **107**, 205–211. The interaction between mistuning and friction in the forced response of bladed disk assemblies.
10. W. D. Iwan 1967 *Journal of Applied Mechanics*, 612–617. On a class of models for the yielding behaviour of continuous and composite systems.
11. H. L. Wettergren and G. Csaba 1996 Dynamic instability of a turbine generator due to microslip. Accepted for publication in *Journal of Vibration and Acoustics*.
12. H. L. Wettergren 1996 Optimal design to reduce dynamic instability of a turbine generator due to microslip. Submitted to *Journal of Sound and Vibration*.
13. K. Y. Sanliturk and D. J. Ewins 1996 *Journal of Sound and Vibration* **193**, 511–523. Modelling two-dimensional friction contact and its application using harmonic balance method.

APPENDIX: NOTATION

A	damper-bar cross-section area
c_{eq}	damping term
[C]	damping matrix
DOF	degree of freedom

E modulus of elasticity
EO engine order of excitation
F traction force on friction joint, blade-to-blade damper force
F_f friction force per unit length
F_{eq} linearized traction force
f_n natural frequency
HBM harmonic balance method
j blade co-ordinate
k stiffness term
[K] stiffness matrix
k_{eq} equivalent stiffness function
k_d damper stiffness between friction joints
l damper-bar length
[M] mass matrix
N number of blades in simulation
n number of blades on disk
P force on platform from dampers
Q excitation force on blade airfoil
q normal load function

Subscript

a amplitude
BB blade to blade
BG blade to ground
eq equivalent linearized property
I Interface
i initial loading
m macro
P platform
u unloading
r reloading

Mathematical symbols

[ ] a rectangular or square matrix
{ } a column vector
$\cdot$ $\mathrm{d}/\mathrm{d}t$
$\wedge$ amplitude value
* a complex quantity
$q_0 q_2$ coefficients for normal load function
s slip direction vector
u friction interface displacement
v damper displacement
w platform displacement
W damping work
x displacement co-ordinate
α, β parameters for Rayleigh damping
β phase angle between excitation and response
Δ slip coefficient
φ interblade phase angle
μ coefficient of friction
ω excitation frequency
ψ mode shape value
θ angular co-ordinate